Ultrasonics Sonochemistry 27 (2015) 72–80

Contents lists available at ScienceDirect

Ultrasonics Sonochemistry

journal homepage: www.elsevier.com/locate/ultson

In situ observation and analysis of ultrasonic capillary effect in molten aluminium

I. Tzanakis [a,*], W.W. Xu [b,c], D.G. Eskin [a], P.D. Lee [b,c], N. Kotsovinos [d]

[a] Brunel Centre for Advanced Solidification Technology, Brunel University, Uxbridge, London UB8 3PH, UK
[b] Manchester X-ray Imaging Facility, University of Manchester, Manchester M13 9PL, UK
[c] Research Complex at Harwell, Didcot OX11 0FA, UK
[d] Laboratory of Hydraulics and Hydraulic Structures, Fluid Mechanics Division, Department of Civil Engineering, Democritus University of Thrace, Greece

ARTICLE INFO

Article history:
Received 3 January 2015
Received in revised form 9 April 2015
Accepted 20 April 2015
Available online 6 May 2015

Keywords:
Sono-capillary
Liquid metal
Cavitation
Micro jet
Oxide
Melt-filtration

ABSTRACT

An in situ synchrotron radiographic study of a molten Al–10 wt% Cu alloy under the influence of an external ultrasonic field was carried out using the Diamond-Manchester Branchline pink X-ray imaging at the Diamond Light Source in UK. A bespoke test rig was used, consisting of an acoustic transducer with a titanium sonotrode coupled with a PID-controlled resistance furnace. An ultrasonic frequency of 30 kHz, with a peak to peak amplitude at 140 microns, was used, producing a pressure output of 16.9 MPa at the radiation surface of the 1-mm diameter sonotrode.

This allowed quantification of not only the cavitation bubble formation and collapse, but there was also evidence of the previously hypothesised ultrasonic capillary effect (UCE), providing the first direct observations of this phenomenon in a molten metallic alloy. This was achieved by quantifying the re-filling of a pre-existing groove in the shape of a tube (which acted as a micro-capillary channel) formed by the oxide envelope of the liquid sample. Analytical solutions of the flow suggest that the filling process, which took place in very small timescales, was related to micro-jetting from the collapsing cavitation bubbles. In addition, a secondary mechanism of liquid penetration through the groove, which is related with the density distribution of the oxides inside the groove, and practically to the filtration of aluminium melt from oxides, was revealed. The observation of the almost instantaneous re-filling of a micro-capillary channel with the metallic melt supports the hypothesised sono-capillary effect in technologically important liquids other than water, like metallic alloys with substantially higher surface tension and density.

1. Introduction

When a liquid volume is subjected to a high-intensity ultrasonic field close to the entry of narrow spaces such as capillaries, canals, pores and voids an abnormally high rise of the liquid is observed inside these narrow channels. This phenomenon is known as the sono-capillary or ultrasonic capillary effect (UCE) and the research was first initiated in the former Soviet Union in early 60's and 70's [1,2]. More recently, UCE attracted the attention of researchers with regard to liquid filtration and impregnation [3]. Several hypotheses regarding the driving mechanism of the UCE have been developed [4–10]. At the same time, a robust theory explaining the driving mechanism of the UCE has not been found yet as there are only few real time observations of UCE available that can provide us with a coherent validation of the existing theories.

Specifically, experimental studies on water showed that the extreme dynamics of the acoustic cavitation bubbles were observed at the entry to capillary tubes, suggesting that cavitation generation is a requirement of the sono-capillary phenomenon assisting the penetration of the surrounding liquid into capillary micro-channels [5]. Dezhkunov et al. [6] showed that in the absence of cavitation no rise of the liquid in a capillary was recorded. As the amplitude of vibrations increased and a cavitation cloud appeared at the capillary channel inlet, the liquid raised inside the capillary, implying that the cavitation activity played a crucial role in the UCE. Additionally, Sankin et al. [7] suggested that the sono-capillary effect might be explained, at least partially, by a counter pressure arising from the bubbly cloud and the capillary interaction. Although they stated that the point of application of the counteracting force influencing the liquid flow in the capillary had yet to be found. In line with these research findings was the recent work of Tamura et al. [8], who suggested that the cavitation bubbles formed at the open end of a capillary tube contribute to

* Corresponding author.

http://dx.doi.org/10.1016/j.ultsonch.2015.04.029
1350-4177/

the pressure accumulation within the tube leading to the raised height of the liquid. In contrast, Rozina et al. [9], proposed that the specific cavitation phenomena (the shock waves and high velocity cumulative jets) were not the decisive factor for the formation of liquid flow penetrating micro-capillary channels and also reported that the process of the filling of dead-end capillaries with a liquid in the ultrasonic field, was affected mainly by the dissolution of gas inside the capillary rather than cavitation [10]. The role of cavitation and cavitation bubble dynamics in the UCE phenomenon therefore remains an open subject for further investigation.

Despite the continuing debate on the mechanisms of the sono-capillary effect, the application of UCE is extremely important for industry as it underlies intensification of many important technological and chemical processes connected with oil production [11], bio-sludge and biomass processing [12], membrane filtration [13], ceramic filters [14], micro-biology [15] as well as advances in metal casting industry and the production of high quality castings [16]. The effects induced by ultrasound in liquid media and their influence on the industrial metal processing have been studied for many years under the umbrella of acoustic cavitation [16,17]. Although these effects are widely used, there is a large room for technology improvement that requires better understanding of the involved mechanisms. In addition to filtration, wetting and impregnation applications, the forced filling of small-scale defects formed during solidification, e.g. grooves, voids, crevices, which could eventually lead to crack formation and propagation, can potentially reinforce the as-cast structure and improve structural integrity of the as-cast metal.

The experimental studies of UCE in liquid metals have been hindered until recently by obvious limitations such as high temperatures, opaqueness and chemical activity of the melts. Nowadays X-ray imaging technology, available through the third generation synchrotron radiation sources, is extensively applied in the in situ and real-time investigations of liquid metals and their solidification processes [18–20].

In the current study, the direct observation of the penetration of a liquid metal into a pre-existing groove (acted as a micro-capillary channel) during the ultrasonic processing of a liquid Al–10 wt% Cu alloy, enabled by the Diamond Light Source – the national synchrotron facility of the UK, is used for testing some of the theoretical approaches behind the UCE. To the best of our knowledge this is the first time when the filling of a capillary with the liquid metal under cavitation conditions has been observed. Our results showed that a possible mechanism responsible for the UCE is the collapsing activity of cavitation bubbles in the vicinity of the micro-capillary inlet. The results are in a good agreement with the hypothesis regarding the cavitation nature of the UCE as reported by Dezkunov and Leighton [5,21–23] who analysed this phenomenon in water. Through this novel research we are now able to help answer the long-stated questions: (a) can ultrasound assist the penetration of capillary channels in the molten metals, (b) what are the governing mechanisms and (c) are these mechanisms related with the local activity of the cavitation bubbles? The discovery of the almost instantaneous re-filling of a micro-capillary channel with the metallic melt is highly important, as it appears to confirm the existence of the sono-capillary effect in technologically important liquids, other than water, like metallic alloys with substantially higher surface tension and density.

2. Methodology

In situ synchrotron X-ray radiography studies of a molten Al–10 wt% Cu alloy subjected to ultrasonic processing were carried out using the Diamond-Manchester Branchline at the Diamond Light Source (National Synchrotron Facility in UK). A bespoke ultrasonic test rig, consisting of an ultrasonic processor coupled with a Ti sonotrode and a PID-controlled resistance furnace (see [24]) was used (Fig. 1a). A split furnace with a small X-ray translucent window to allow the X-rays to pass with minimal attenuation was vertically aligned with the direction of the X-rays as shown in Fig. 1b. A specially developed crucible made of BN (boron nitride) was placed in the centre of the furnace and in line with the window. The BN crucible (key dimensions shown in Fig. 1b) was used due to its low X-ray attenuation compared to the Al–Cu alloys, and the thickness of the crucible cavity where X-rays penetrate through was 1 ± 0.05 mm. The Al–10 wt% Cu alloy was pre-machined in order to fit into the cavity of crucible. The alloy was then melted and stabilized at 660 ± 10 °C. The temperature

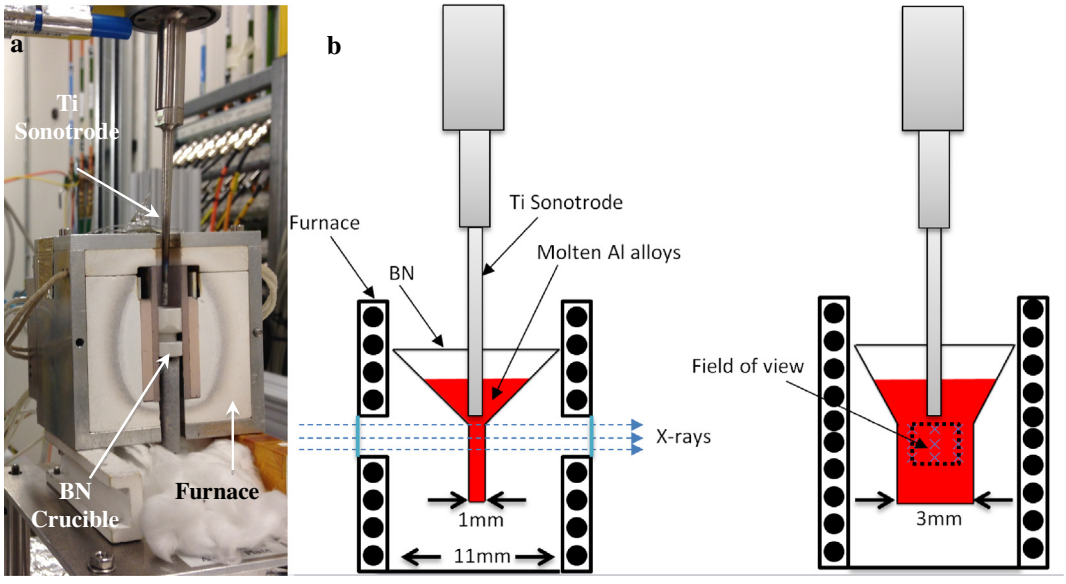

Fig. 1. Experimental test rig: (a) sectional view of the experimental set up and (b) schematic representation of the test rig with some key dimensions of the furnace and BN crucible used for the ultrasonication in the beamline. The high density X-ray beam is delivered through the X-ray tube to the molten sample placed inside the crucible. The camera on the opposed side captures the real time event of ultrasonication and delivers images to the super-computer for further analysis.

Table 1
Characteristic properties of Al–10 wt% Cu.

Properties of an Al–10 wt% Cu alloy	
Liquidus (°C)	630
Density (kg/m^3)	2600 [25]
Viscosity (mPa s)	2.3 [26]
Speed of sound (m/s)	4725 [27]

was measured by a K-type thermocouple submerged into the liquid melt. Characteristics of the melt alloy can be found in Table 1.

This entire sample holder arrangement could be moved vertically so that, as acoustic cavitation is being developed, the position of the region of interest could be manipulated with respect to the X-ray beam and the imaging camera. To produce ultrasound and consequently cavitation bubbles a 50-W ultrasonic piezoelectric transducer (Hielscher UP50H) was deployed. The Ti sonotrode with a tip diameter of 1 mm was immersed to a depth of ~4 mm in the melt. The use of a Ti sonotrode was justified by the short term exposure to the melt. A constant peak-to-peak amplitude of 140 μm and a frequency of 30 kHz were maintained (performance data of the ultrasonic processor was received from the manufacturer – Hielscher). The transducer generated an intensity of 93.8 W/mm^2 and a pressure of 16.9 MPa at the 1 mm radiation face, calculated using the analytical model in [28]. The duration of the test was 30 s and recordings of bubbles dynamic performance were collected for various time ranges.

The high flux pink X-ray beam passing through the sample was recorded with a PCO-Edge camera. The camera with a field of view of 2.1 × 1.8 mm^2 was used to collect images with pixel size (at the sample) of 0.81 μm. The 0.025 s exposure time was adopted in this study and the final image frame rate of $1/(0.025 + 0.053) \approx 13$ fps was obtained while the average overhead time in the data acquisition process was 0.053 s per frame. In addition, the sonication pulse was generated in a way such that the power was charged for 0.5 s then discharged for 0.5 s in every 1.0 s (i.e., the cycle is 1.0 s). The working distance between the scintillator and the sample was adjusted to 7.5 cm to achieve some in line phase contrast.

3. Results and discussion

Solid aluminium is normally covered with a thin oxide film that is strong and thermally stable with a thickness of 2–30 nm [29]. This oxide film can become thicker on heating the solid metal in air. As a result, the molten alloy inside the experimental crucible was enveloped by an oxide film that might contain irregularities like micro-channels, folds and grooves. Fig. 2 (see white arrow) shows such an irregularity with characteristic dimensions of 850 μm length and an average width of 25 μm. This particular feature happened to be in the field of view just below the sonotrode and at a vertical distance of about 0.5 mm from its tip. In this study the abrupt change of a contrast of this feature (called "groove" hereafter) during ultrasonic processing is discussed and linked to a capillary behaviour.

In the series of synchrotron radiation X-ray images in Fig. 2 a cloud of cavitation bubbles in the melt was observed near by the top entrance of the studied groove. Cavitation bubbles of different sizes can be clearly distinguished by the sharp contrast between bubbles and the melt, most of the bubbles are concentrated near the radiation face of the sonotrode, and became scattered and smaller with distance away from the sonotrode tip [19]. These bubbles are mainly formed by the dissolved gases, mostly hydrogen, released from the melt due to the applied external forces from the ultrasonic transducer. When the amplitude of the acoustic pressure exceeds a threshold (e.g. ~0.7 MPa for molten aluminium for frequencies around 20 kHz and for a particular gas and inclusions content) then cavitation bubbles are formed [16]. Some of these bubbles may pre-exist in the melt before the ultrasonic processing has started [18], originating from entrapped air or residual moisture in the porous BN crucible or in double-oxides in the melt. Consequently, upon crossing the cavitation threshold there is a transition to a regime of developed cavitation, when all bubbles rapidly expand during the half period of rarefaction. The pressure inside the cavitation bubble becomes much lower than the static ambient pressure, so the bubbles start to violently collapse during the subsequent compression half periods, generating high-speed liquid jets and shock waves. The initial velocity of the produced high-speed jets, with a typical diameter about 1/10 of the maximum bubble diameter, vary from 300 to 1000 m/s while the corresponding local hydrodynamic impact pressures usually lie between 0.2 and 2 GPa according the experimental results in [30] but can also be as high as 10 GPa in some cases [31,32]. These high-speed jets are supposed to overcome the capillary pressure in channels/grooves and allow the liquid metal to pass through easily.

The observations in Fig. 2 show that the groove which was hidden in the background for up to 10 s, instantaneously (between consecutive frames) changes its contrast to brighter and then stays with the same contrast and geometry for many ultrasonic pulses. The interpretation of this observation can be hypothesised in different ways. The brighter (lighter) contrast means that the X-rays experience less absorption on their path so the contents of the groove should change from background material (aluminium alloy melt) to something less absorbing.

There is a choice of such substances. Aluminium oxide has about 40% less (1.8×10^4 eV) photon energy absorption potential as compared to the Al–10 wt% Cu alloy (2.9×10^4 eV) and the gases (hydrogen, air) absorb much less energy than solid and liquid phases [33] (that is why the gas-filled cavitation bubbles have the brightest contrast, see red arrow in Fig. 2a). An aluminium melt always contains submicron oxide particles [16], also oxide films can easily break to individual particles typically between 0.5 and 1.5 μm in size [34]. Moreover, oxides are formed around the gas cavitation bubbles giving them a slightly darker rim. Gases like H_2, which can be found in the surrounding atmosphere in a form of free gas or water vapour, are absorbed and dissolved into the aluminium melt and facilitate the cavitation acting as nuclei [16].

The nature of the groove is also debatable and different possible scenarios are shown schematically in Fig. 3. It may come to existence as groove at the external oxide envelope that under the action of oscillating liquid phase pops in the interior of the melt as shown in Fig. 3a. In such a case the convex groove filled with liquid becomes a concave groove filled with gas and therefore appears brighter. The other possibility is that the groove convex initially filled with the melt acts as a site for precipitation of hydrogen porosity, accelerated by cavitation activity. In this case, a hydrogen bubble (or several coalesced bubbles) precipitate at the alumina surface of the groove and spread along its surface forming an elongated gas pocket, Fig. 3b. Yet another possibility is that the external oxide envelope experiencing oscillations fold onto itself locally forming a bi-film tube-like groove filled with liquid as shown in Fig. 3c. This explains why it blends with the background initially. The change in the contrast results from the cavitation activity that forces the liquid through this tube accompanied (as will be argued below) with sedimentation of oxide particles or gas inside the tube.

It is worth to note here, that although the groove becomes brighter it seems to be less bright than the gas-filled bubbles. The first and second mechanisms of groove formation assume that the changes in the groove orientation (Fig. 3a) or contents

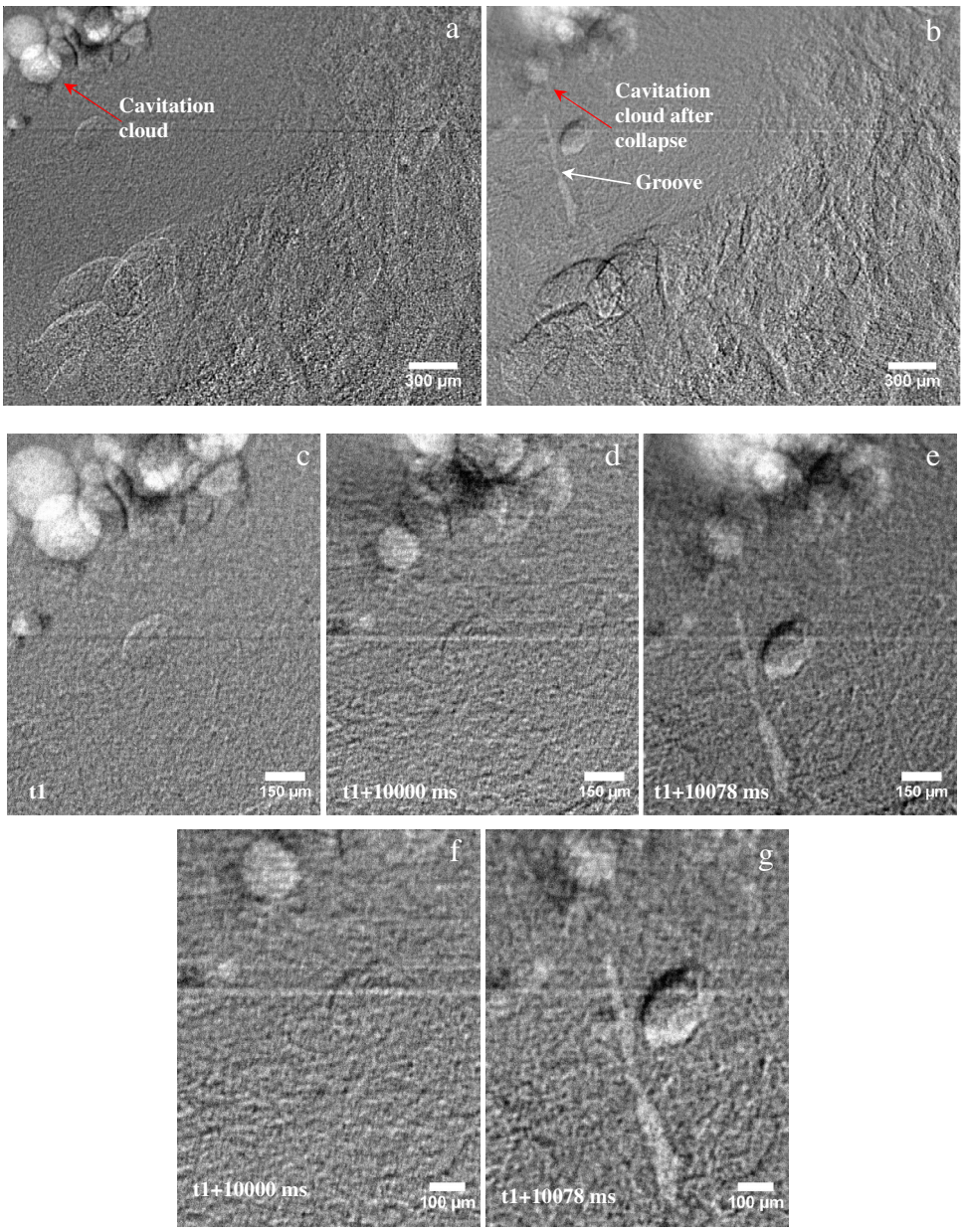

Fig. 2. Radiographs of the pre-existing groove (white arrow) which (a) is filled by liquid melt until the moment when (b) refill takes place and the groove is revealed. The bubbly cavitation cloud on top (red arrow) is also shown. A series of images showing (c) the groove in the beginning of the experiment at t1 with the majority of active cavitation bubbles in a distance of 200–300 μm from the groove inlet, (d) the time moment just before the re-filling process after about 10 s of ultrasonic processing and (e) the re-filling process of the groove, activity from cavitation bubbles (powerful collapses) at the inlet of the groove pushed the bulk fluid towards the groove. Zoomed in views clearly show the state (f) before (hidden) and (g) after (revealed) the re-filling of the groove highlighting the sono-capilary effect. (For interpretation of the references to colour in this figure legend, the reader is referred to the web version of this article.)

(elongated gas bubble, Fig. 3b) commonly happen under the oscillating conditions imposed onto the oxide envelope. The oscillations induce turbulence in the liquid phase and should be felt throughout the sample with the events matching the first two scenarios occurring rather frequently. We, however, have not observed anything like that throughout a series of similar experiments. Also in these two cases the oscillations of the liquid should reflect the change of geometry of the groove. The contrast and geometry of the groove, however, remains the same for a very long time (on the scale of vibration frequency and frame rate). This leaves us with the suggestion that our observation is a result of several events that happen to occur in the right place at the right time, making them possible but not common. The third case gives us a rather rigid structure (an external oxide skin folded inside to form a bi-film tube [35]) that is not common but quite possible (Fig. 3c). Additionally, the probability of this mechanism happening on the pathway of X-rays is relatively small so we have not observed this phenomenon frequently. This case also assumes that the mechanisms resulting in the contrast change are triggered by the cavitation activity of the bubbles accumulated close to the inlet of the tube, which does require some coincidence. The contrast changing in this bi-film tube is hypothesized to be due to the forced through-flow of the melt with entrained oxide particles or gas enabled by high-speed jets from bubbles collapsing close to the one end of the tube. Below this mechanism is explained in more detail. Before going further we need to note that all three mechanisms are possible, we just think that the third one is more likely to fit all the observations in our experiment.

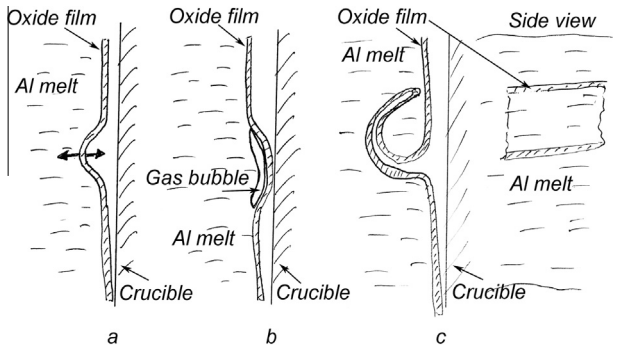

Fig. 3. Schematic representation of different scenarios leading to the appearance of the observed phenomenon: (a) oxide film which pops into the Al–Cu melt due to the ultrasonic vibration of the melt to form a concave groove, the length of the X-ray pathway trough the melt is reduced and a brighter in contrast area should be revealed; (b) an elongated gas bubble formed inside the convex groove, effectively leading to the same contrast change as in (a); and (c) a tube-like groove formed by a folded oxide film filled with the melt, side view shows that the groove is opened from two sides. Oscillating and collapsing cavitation bubbles at the entry to the tube force the melt with the entrained oxide particles or gas through the groove, whereas gas or oxide particles sediment inside the groove causing the change in the absorption contrast.

If we assume that a single bubble collapses on average every 33 μs (a full acoustic cycle), then there are potentially 2500 collapse events happening within each time-frame of 78 ms. Thus, the chances of numerous projectile micro-jets targeting the opening of the tube are very high. As the aluminium melt inevitably contains microscopic oxide particles and oxide films, those will be entrained by the liquid jet, acquire momentum and move into the tube along with the melt. In a repeated action of melt being pushed through the tube by collapsing cavitation bubbles, oxide particles accumulate in the groove (due to their higher mass density than the surrounding liquid) causing the change of the contrast (Fig. 2).

Thus, the difference in contrast after the re-filling process reveals the secondary effect of the liquid penetration through the groove, apart from the filling mechanism, which is related with the density distribution of the oxides inside the groove, and practically to the filtration of aluminium melt from oxides. Eventually the observation in Fig. 2 can be explained as follows:

(a) Initially, the tube-like groove is filled with the matrix alloy (Fig. 3c) and the composition of the melt and the concentration of oxides in the groove are the same as in the bulk melt. Thus, the contrast remains the same and tube blends with the background.
(b) The jet with a finite volume V_{jet} from a collapsing cavitation bubble (or a series of collapsing bubbles) at the entry of the tube entrains the bulk liquid, which is a mixture of the Al–Cu alloy and oxides.
(c) Due to high momentum created by cavitation bubble implosion, the liquid jet with the volume V_{jet} enters the tube.
(d) Due to mass continuity, the jet pushes the liquid/oxide mixture within the tube and the corresponding mass of the original liquid with the same volume is displaced out of the tube.
(e) The concentration of oxides inside the tube-like groove increases due to the settling and capturing of oxide particles (as explained in more detail below, see Eq. (14)).
(f) A sequential number of such events can force substantial amounts of liquid melt through the groove; therefore, the concentration of oxides in the groove increases further.

A similar explanation was given by Ohl et al. [36] where they used high intensity focused ultrasound to deliver antibacterial nanoparticles into simulated tubular dental channels with similar aspect ratio to the studied groove and the oxide particles. They experimentally showed that the bubbles collapsing at the opening of tubular dental micro-channels were able to propel nanoparticles along the whole length of the channel due to the pressure associated with the high speed micro-jets, covering a large percentage of those channels with nanoparticles. In line with these results was also the work by Pavard et al. [37] where they demonstrated the importance of the high speed micro-jet in pushing liquid and microparticles through a capillary tube (open in both ends) even when the cavitation bubbles were generated far away from the entrance of the capillary tube.

Let us now justify these propositions by some analytical calculations that can prove that the liquid jets from imploding bubbles are able to overcome the capillary pressure in channels/tubes and allow the liquid metal to pass through. In this stage we need to mention that since that tube-like groove was revealed after 10 s of sonication time, the acoustic pressure (16.9 MPa) generated by ultrasonic waves cannot be responsible for that filling.

Initially, in order to understand the mechanism of the forces which push the Al–Cu melt through the tube, the liquid jet dynamics was calculated according to [38].

The momentum flux F (jet force) is defined as follows:

$$F = \rho(M_0) \tag{1}$$

where ρ is the liquid density of the Al–Cu alloy and M_0 is the initial kinematic momentum flux which is defined as:

$$M_0 = \int_A U^2 dA = \pi R^2 U_0^2 \tag{2}$$

where R is the initial jet radius and U_0 is the initial jet velocity.

Then the pressure, P_{jet}, exerted by the jet force at the entrance of the tube is given by the relation:

$$P_{jet} = \frac{F}{A_j} = \frac{F}{\pi b^2/4} = \frac{F}{\pi (c_1 x)^2} \tag{3}$$

where A_j is the area of the jet cross section at the distance x, $b = 2c_1 x$ is the typical jet diameter at distance x, and c_1 is the experimental jet expansion coefficient equal to 0.15 [38]. The initial jet kinematic mass flux $\mu_0(x)$ (i.e. volume flux) is equal to

$$\mu_0 = \pi R^2 U_0 \tag{4}$$

while the jet kinematic mass flux $\mu(x)$ arrives at the entrance of the groove is related with the jet kinematic momentum flux M_0:

$$\mu(x) = f(m, x) = cx\sqrt{M_0} \tag{5}$$

where c is an experimental constant equal to 0.25 [38].

The duration (i.e. lifetime) of the jet Tjet, emerging from the implosion of a single bubble is approximately equal to the travel time of the jet (emerging from the imploding bubble with initial jet velocity U_0) to reach the inlet of groove at distance x. Therefore the duration of the jet Tjet is approximately equal to the ratio of the distance x to the initial jet velocity U_0. The liquid volume $\mu'(x)$ which reaches the entrance of tube (groove) during jet's lifetime is given by:

$$\mu'(x) = \mu(x) T_{jet} \tag{6}$$

The calculations for the above jet parameters are shown in Table 2, assuming distance x of the jet from the inlet of the tube-like groove at 30 μm (almost touching the tube inlet) to a distance of 300 μm (assumed a maximum typical distance according to the location of the cavitation bubbles in Fig. 2), jet diameters from 3 to 12 μm (as according to our previous study, using exactly the same equipment, the majority of cavitation bubbles in the Al–Cu melt are found in the range of 15–60 μm in radius [19] so as

Table 2
Cavitation liquid jet dynamics: calculations of hydrodynamic pressure exerted by the jet and the kinematic mass flux of the jet for various bubble sizes, jet velocities and distances from the groove entrance were performed.

$2R$, diameter of jet (cm)	U_0, initial jet velocity (cm/s)	$\mu_0(x)$, initial jet kinematic mass flux (cm^3/s)	M_0, jet kinematic momemtum flux (cm^4/s^2)	x, distance of jet origin from upper side of the groove (cm)	b, jet diameter at distance x (cm)	F, jet force (N)	A_j, jet area at groove (cm^2)	P_{jet} pressure exerted by the jet at the entrance of the groove (MPa)	$\mu(x)$, jet kinematic mass flux (cm^3/s)	T_{jet}, jet duration (s)	$\mu'(x)$, jet volume at groove entrance during jet life (cm^3)
0.0003	30000	0.002	63.6	0.03	0.009	1.65E−03	6.4E−05	0.3	0.06	1.00E−06	5.98E−08
0.0012	30000	0.034	1017.4	0.03	0.009	2.65E−02	6.4E−05	4	0.24	1.00E−06	2.39E−07
0.0003	100000	0.007	706.5	0.03	0.009	1.84E−02	6.4E−05	3	0.20	3.00E−07	5.98E−08
0.0012	100000	0.113	11304.0	0.03	0.009	2.94E−01	6.4E−05	46	0.80	3.00E−07	2.39E−07
0.0003	30000	0.002	63.6	0.003	0.0009	1.65E−03	6.4E−07	26	0.01	1.00E−07	5.98E−10
0.0012	30000	0.034	1017.4	0.003	0.0009	2.65E−02	6.4E−07	416	0.02	1.00E−07	2.39E−09
0.0003	100000	0.007	706.5	0.003	0.0009	1.84E−02	6.4E−07	289	0.02	3.00E−08	5.98E−10
0.0012	100000	0.113	11304.0	0.003	0.0009	2.94E−01	6.4E−07	4622	0.08	3.00E−08	2.39E−09

mentioned before in the beginning of this section the effective jet radius should be about 1/10th of the maximum) and initial jet velocities U_0 from 300 to 1000 m/s.

Note that the pressure delivered by the jet at the inlet of the tube depends on the distance of the imploding bubble from the tube and from the aggressiveness of the bubble which is determined by the initial jet velocity and jet diameter. Using a combination of initial parameters, based on estimations from our experimental observations, it can be seen from Table 2, that the pressure can reach very high values, from less than 1 MPa up to more than 4 GPa. This pressure is several orders of magnitude higher than the capillary pressure in the case when the tube is initially filled with air, which is higher than when the tube is filled with the same liquid. This maximum capillary pressure is 0.135 MPa at a contact angle of 140° according to the following expression [16]:

$$H = \frac{4\sigma\cos(\theta - 90^\circ)}{\rho g d} \tag{7}$$

where H is the metallostatic head required for the melt to pass through the capillary, σ is the surface tension, ρ is the melt density, d is the capillary diameter, θ is the contact angle, and g is the gravity acceleration. Thus, the pressure jet exerted from the collapse of a bubble near the entrance of the tube-like groove can easily overcome this pressure barrier and fill the groove with the Al–Cu melt.

As shown from Table 2, the jet kinematic mass flux (i.e. the jet volume flux) $\mu(x)$ increases with distance from the jet origin (i.e. bubble implosion), so increases the area of the jet at any cross section perpendicular to jet axis. The jet force (F) is constant but the pressure ($P_{jet} = F/A_j$) at any cross-section decreases substantially with increasing distance from the jet origin. When a bubble is further away, i.e. 300 μm, the jet arrives at the groove with a larger cross-section and with a smaller pressure, hence the transfer of mass to the groove is reduced. The mass transfer to the groove can be even zero if the pressure is not high enough to overcome the friction within the groove. The exerted pressure at the groove inlet is the critical parameter, which forces the mass into the groove. It is observed from Table 2 that the pressure is higher for short distances.

Let us consider the flow within the tube-like groove, and for simplicity we approximate the tube by two parallel rigid planes 25 μm apart. For this geometry, the fluid moves in the x direction parallel to the plates, assuming that there is no velocity in the y or z directions. The driving force of the Al–Cu flow in the tube is the pressure gradient between the upper and lower end of the tube. A first approximation is to assume that the flow is laminar.

It is suggested in the literature that the typical period of time for a single oscillation of an aluminium cavitation bubble with a maximum radius of ~100 μm is in the order of ~50 μs predicted by using classic Gilmore model [20]. Thus, we advocate that the filling of the groove can be accomplished in a very short time Δt. For that reason we have chosen typical time periods related to the oscillation of a non-linear bubble (50 μs), to the collapse of typical cavitation bubbles (1–2 μs) [39,40] and some additional times close to the latter (3–5 μs). In order to have a complete analysis and logical understanding of the groove filling mechanism we also decided to investigate different time steps: at 33 and 16.5 μs which is the full and the half acoustic cycle from the ultrasonic source, respectively. In such a way we will be able to answer the question on which mechanism (according the pressure acquired to fill the groove, see Table 3) is responsible for that filling i.e. the high speed micro-jet during bubble collapse, the acoustic pressure emissions during bubble oscillation, or the acoustic field during the movement of the sonotrode.

Knowing the characteristic dimensions of the tube (850 μm in length and 25 μm in width), the mean velocity of the liquid melt within the tube during the filling time of Δt can be found by the following expression $U_{mean} = l/\Delta t$ where l is the length of the groove. The Reynolds number of the flow inside the groove can be estimated as follows:

$$\mathrm{Re} = \frac{\rho U_{mean} d}{\mu} \tag{8}$$

where ρ is the density of the melt, U_{mean} is the mean velocity, d is the characteristic width of the tube and μ the dynamic viscosity of the melt. This Reynolds number indicates that in time steps larger than 10 μs (Re < 2400) the flow within the groove can be considered as laminar. However, the basic idea of the filling mechanism will be not changed, if we assume that the flow in the tube is turbulent as

Table 3
Analytical calculations of the amount of hydrodynamic pressure required to fill the tube-like groove at different time steps. Filling can be accomplished in time steps below 3 μs.

Time of filling the groove (s)	Mean velocity of the flow profile filling the groove (m/s)	Max velocity of flow profile filling the groove (m/s)	Required pressure to fill the groove (MPa)
5.00E−05	17.0	34.0	1.3
3.30E−05	25.8	51.5	1.9
1.65E−05	51.5	103.0	3.9
5.00E−06	170.0	340.0	12.8
4.00E−06	212.5	425.0	16.0
3.00E−06	283.3	566.7	21.3
2.00E−06	425.0	850.0	31.9
1.00E−06	850.0	1700.0	63.8

in the case of a very short period of time, i.e. 1 or 2 μs, Re can be as high as 24,000.

For steady, laminar flow between fixed parallel plates there is an analytical solution of the flow, described by the Navier–Stokes equations. The solution regarding the velocity profile within the groove is given by the following equation [41]:

$$u(y) = \frac{p(0) - p(l)}{2\ \mu l} y(d - y) \tag{9}$$

where y is Cartesian coordinate perpendicular to the assumed rigid plane of the groove, $p(0)$ and $p(l)$ the pressure at the upper and lower end of the groove. For $y = 0$ and $y = d$, the velocity $u(y)$ vanishes (non-slip condition).

The maximum velocity U_{max} within the groove is obtained for $y = d/2$ as:

$$U_{\max} = \frac{p(0) - p(l)}{8\ \mu l} d^2 = \frac{\Delta p}{8\ \mu l} d^2 \tag{10}$$

where $\Delta p = p(0) - p(l)$. The mean velocity U_{mean} within the groove is expressed by the following equation:

$$U_{\text{mean}} = \frac{2}{3} U_{\max} \tag{11}$$

Thus by substituting Eqs. (10) and (11) and solving for Δp, the required pressure to accomplish the groove filling is obtained as:

$$\Delta p = \frac{12\ \mu l}{d^2} U_{\text{mean}} \tag{12}$$

Results using the above calculations for different time steps can be found in Table 3.

Considering the fact that the bi-film tube-like groove, pre-existed for a significant period of time (>10 s) without any changes, it is very unlikely that the acoustic pressure of 16.9 MPa developed at the sonotrode tip is responsible for the observed phenomenon. This pressure is still much higher than 3.9 MPa which would be required to fill the tube at the filling time of 16.5 μs (corresponds to the half positive cycle displacement of the sonotrode) or even at 5 μs when the required pressure is at 12.8 MPa (Table 3). As no changes in the contrast happened under general sonication conditions until the cavitation bubbles appeared close to the tube, the filling hardly happened at these time scales. Thus, the filling of the groove would require even shorter times, less than 5 μs, corresponding to pressures higher than 16.9 MPa. Such a high pressure implies involvement of collapsing cavitation bubbles. Apparently, the required pressure to fill the groove is within the range of pressures exerted by the jet from collapsing bubbles (see Table 2). We already mentioned, that the acting bubbles are most likely to be those at about 200–300 μm from the entrance of the groove, as seen by Fig. 2. The pressure delivered by the high speed micro-jet at the inlet of the groove after the collapse of bubbles at a distance of 300 μm from that inlet is in the range of 0.3–46 MPa (Table 2) which, on the upper side, is enough to fill the groove. The bubbles which implode at such distances from the groove, entrain ambient fluid and reach the groove with a volume flux $\mu(x)$ about 10–30 times larger than the initial volume flux $\mu_0(x)$ (see Table 2), which implies that also a large number of entrained oxides are forced to enter the groove, enhancing the increment in the number of oxides within the groove (discussed in Fig. 3) in a shorter time.

The calculated pressures in Table 3 are in a good agreement with the calculations in Table 2 where the required pressure for filling the groove is in the same range with the calculations of the hydrodynamic impact pressure delivered by the micro-jet at the entrance of the groove, hence transport of liquid mass and oxide particles inside the groove will occur.

Finally, we check the hypothesis about oxide particle accumulation. For a certain size r_s, which are determined by the Stokes number (Eq. (13)), particles no longer move with streamlines. Inertia (viscosity, gravity) plus the jet momentum tend to straighten the trajectories of these particles in those points where the stream changes its direction. As a result, the probability of a particle being retained by the tube significantly increases. This mechanism is called inertial impaction and is well explained in [16,42].

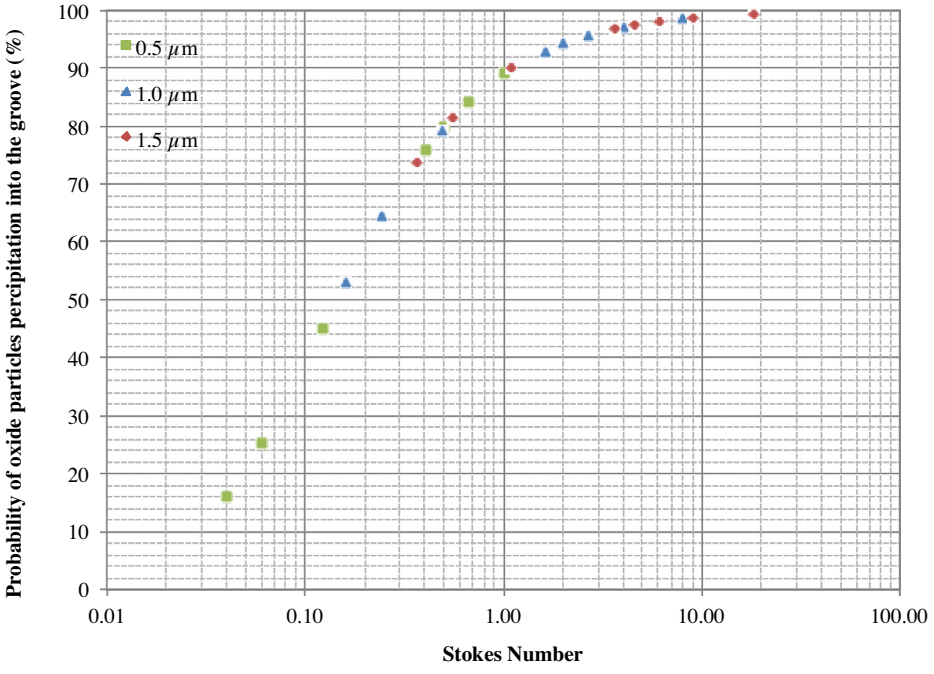

Fig. 4. Probability of three different sizes (0.5, 1 and 1.5 μm) of Al oxide particles precipitate into the groove as a function of the Stokes number.

Under conditions of potential melt flow (see Table 3) within the groove (Re = 400 – 24,000) driven by the collapse of the bubble clouds nearby the entrance of the groove, particles will precipitate on the filter in the groove if [16]:

$$\mathrm{Stk_{cr}} = \frac{2\mathrm{Re}\rho_m r_s^2}{9\rho_i R^2} \geqslant 0.08 \quad (13)$$

In the case of potential flow, the probability of a particle being precipitated in inertial impact is determined as [16]:

$$E_i = \frac{\mathrm{Stk}^2}{(\mathrm{Stk}+0.06)^2} \quad (14)$$

For the critical value of Stk = 0.08 (Eq. (13)), the probability of precipitation $E_i = 0.33$. Hence, only one third of inclusions with critical and larger sizes can be accumulated by inertial impact inside the groove.

Fig. 4 gives the probability of particles capture (E_i, Eq. (14)) in the tube for various oxide particle sizes and Stokes numbers (Eq. (13)). It is obvious that for Al oxide particles with a typical diameter between 0.5 and 1.5 μm and for the time of filling the tube between 50 and 1 μs which is tied up with the collapse of bubbles (see Table 3), the precipitation percentage of particles inside the tube varies from 13.5% to 99.2%. In particular, for smaller particles of 0.5 μm in diameter, the precipitation percentage inside the groove varies from 13.5% to 93.5%. For particles with a size of 1 μm the precipitation probability is higher, from 48.7% up to 98.3%; while for even larger particles of 1.5 μm in size, the precipitation percentage varies from 70.4% up to 99.2%. Consequently, these results in combination with the number of collapsing events in the frame rate window of 78 ms and the volume of melt and oxides carried out by the jet inside the tube (Table 2) clearly show that the precipitation of Al oxides inside a capillary is a process that is tied up with the collapse of bubbles and particularly with the distance of the incoming high speed jet from the entrance of the groove, the speed of the jet, the size of the jet and the duration of the filling. This mechanism is also related with the ultrasonic melt filtration [16]. Results are in a very good agreement with the studies in [36] where the physical mechanism of particle delivery inside a capillary tube due to the action from the high speed micro-jet was experimentally shown.

4. Conclusions

Very few studies of the ultrasonic capillary effect (UCE) in liquid metals have been performed due to the complex nature of the physical processes involved. This lack of real-time observations, due to the challenges of high temperature experimentation and opaqueness of the melts, has restricted the validation of existing UCE theories.

In this study, the re-filling of a pre-existing oxide film tube-like groove, with the action of ultrasound upon an Al–Cu melt was monitored. Analytical solutions of the hydrodynamic impact pressure exerted from the cavitation implosion jet and the hydrodynamic pressures required to fill the studied groove, have shown that the mechanism responsible for the re-filling of the groove with the melt is the collapse of cavitation bubbles near by the groove inlet. This is important evidence that clarifies for first time ever the existence of UCE in liquid metals.

Additionally, during the re-filling mechanism, a secondary effect is also revealed from the changing contrast of the X-ray synchrotron images. It was shown that the concentration percentage of oxides, that are captured in the groove during melt flow through it, is likely to increase. The precipitation of Al oxides inside the groove is a process related to the collapse of bubbles and particularly to the distance of the incoming high speed melt jet from the inlet of the tube-like groove, the speed of the jet, the size of the jet and the duration of the filling. The observed phenomenon is related to the ultrasound-assisted filtration of the melt from oxide inclusion.

Acknowledgements

The authors wish to acknowledge financial support from the ExoMet Project which is co-funded by the European Commission in the 7th Framework Programme (contract FP7-NMP3-LA-2012-280421), by the European Space Agency and by the individual partner organisations, the UK Engineering and Physical Sciences Research Council (EPSRC) (EP/K005804/1 and EP/I02249X/1) and the Research Complex at Harwell.

References

[1] E.G. Konovalov, I.K. Germanovich, The ultrasonic capillary effect, Dokl. Akad. Nauk Belorus. SSR 6 (8) (1962) 492–493.
[2] Yu.P. Rozin, V.S. Tikhonova, M.N. Kostucheck, About extremely high constant pressures in the capillary placed close to ultrasonic emitter, Ukr. J. Phys. 20 (1975) 214–220.
[3] T. Matsunaga, K. Ogata, T. Hatayama, K. Shinozaki, M. Yoshida, Effect of acoustic cavitation on ease of infiltration of molten aluminium alloys into carbon fiber bundles using ultrasonic infiltration method, Compos. A 38 (2007) 771–778.
[4] P.P. Prokhorenko, N.V. Dezhkunov, G.E. Konovalov, Ultrasonic Capillary Effect, Minsk, Nauka i Tekhnika, 1981.
[5] N.V. Dezhkunov, T.G. Leighton, Study into correlation between the ultrasonic capillary effect and sonoluminescence, J. Eng. Phys. Thermophys. 77 (2004) 53–61.
[6] N. Dezhkunov, D. Valerio, Physical backgrounds for application of power ultrasound in fluorescent dye penetrant inspection, Forum Acousticum, Budapest, 2005.
[7] G.N. Sankin, N.V. Malykh, Force acting on a cylinder under ultrasonically induced cavitation, Tech. Phys. 50 (7) (2005) 918–923.
[8] S. Tamura, M. Hatakeyama, The role of acoustic cavitation in liquid pressurization in narrow tubes, J. Appl. Phys. 113 (2013) 144905.
[9] E.Yu. Rozina, Yu.P. Rosin, About the nature of the sound capillary pressure, XIII Session of the Russian Acoustical Society, Moscow, 2003. 25–29.
[10] E.Yu. Rozina, Effect of pulsed ultrasonic field on the filling of a capillary with a liquid, Colloid J. 64 (2002) 359–363.
[11] V.O. Abramov, M.S. Mullakaev, A.V. Abramova, I.B. Esipov, Timothy J. Mason, Ultrasonic technology for enhanced oil recovery from failing oil wells and the equipment for its implementation, Ultrason. Sonochem. 20 (2013) 1289–1295.
[12] X. Yin, P. Han, X. Lu, Y. Wang, A review on the dewaterability of bio-sludge and ultrasound pretreatment, Ultrason. Sonochem. 11 (2004) 337–348.
[13] H.M. Kyllonen, P. Pirkonen, M. Nystrom, Membrane filtration enhanced by ultrasound: a review, Desalination 181 (2005) 319–335.
[14] P. Pirkonen, A. Gronroos, J. Heikkinen, B. Ekberg, Ultrasound assisted cleaning of ceramic capillary filter, Ultrason. Sonochem. 17 (2010) 1060–1065.
[15] J.J. Hawkes, M.S. Limaye, W.T. Coakley, Filtration of bacteria and yeast by ultrasound-enhanced sedimentation, J. Appl. Microbiol. 82 (1997) 39–47.
[16] G.I. Eskin, D.G. Eskin, Ultrasonic Treatment of Light Alloy Melts, Second ed., CRC Press, Boca Raton, 2014.
[17] O.V. Abramov, High Intensity Ultrasonic, Gordon and Breach Science Publishers, Amesterdam, 1998.
[18] P.D. Lee, S. Sridhar, Direct observation of the effect of strontium on porosity formation during the solidification of aluminium-silicon alloys, Int. J. Cast Metals Res. 13 (2000) 185–198.
[19] W. Wu, I. Tzanakis, P. Srirangam, S. Terzi, W. Mirihanage, D.G. Eskin, P. Lee, In situ Synchrotron Radiography of Ultrasound Cavitation in a Molten Al–10Cu Alloy, Hoboken (NJ), Wiley/TMS, 2015. TMS2015 Annual Meeting Supplemental Proceedings, pp.61–66.
[20] H. Huang, D. Shu, Y. Fu, J. Wang, B. Sun, Synchrotron radiation X-ray imaging of cavitation bubbles in Al–Cu alloy melt, Ultrason. Sonochem. 21 (2014) 1275–1278.
[21] N. V. Dezhkunov, Ultrasonic Capillary Effect: Theory, Experiment, and Perspectives of Application, in: Proc. 11th All-Union Acoust. Conf., Section N, Moscow, 1991, pp. 135–138.
[22] N.V. Dezhkunov, P.P. Prokhorenko, Dependence of the ultrasonic effect on liquid lift in a capillary on liquid properties, J. Eng. Phys. 39 (1980) 513–519.
[23] N.V. Dezhkunov, T.G. Leighton, The use of capillary as a sensor of cavitation, in: Rudenko, O.V., Sapozhnikov, O.A. (Eds.), Nonlinear acoustics at the beginning of the 21st century. 16th International Symposium on Nonlinear Acoustics ISNA-16 Moscow, Russia, Moscow State University, Faculty of Physics, 2002, 1163–1166.
[24] K.M. Kareh, P.D. Lee, R.C. Atwood, T. Connolley, C.M. Gourlay, Revealing the micromechanisms behind semi-solid metal deformation with time-resolved X-ray tomography, Nat. Commun. 5 (2014) 4464.

[25] A.E. Vol, Handbook of Binary Metallic Systems, Structure and Properties, vol. 1, Israel Program for Scientific Translations Ltd., Jerusalem, 1967. translated from Russian, p. 93.
[26] M. Schick, J. Brillo, I. Egry, B. Hallstedt, Viscosity of Al–Cu liquid alloys: measurement and thermodynamic description, J. Mater. Sci. 47 (2012) 8145–8152.
[27] V.M. Denisov, V.V. Pingin, L.T. Antonova, S.A. Istomin, E.A. Pastukhov, V.I. Ivanov, Aluminium and its alloys in the liquid state, Ural Division Russ. Acad. Sci. (2005) 9. Yekaterinburg.
[28] M.M. Iersel, N.E. Benes, J.T.F. Keurentjes, Importance of acoustic shielding in sonochemistry, Ultrason. Sonochem. 15 (2008) 294–300.
[29] L.P.H. Jeurgens, W.G. Sloof, F.D. Tichelaar, E.J. Mittemeijer, Structure and morphology of aluminium-oxide films formed by thermal oxidation of aluminium, Thin Solid Films 418 (2002) 89–101.
[30] I. Tzanakis, D.G. Eskin, A. Georgoulas, D. Fytanidis, Incubation pit analysis and calculation of the hydrodynamic impact pressure from the implosion of an acoustic cavitation bubble, Ultrason. Sonochem. 21 (2014) 866–878.
[31] E.A. Brujan, T. Ikeda, Y. Matsumoto, On the pressure of cavitation bubbles, Exp. Therm. Fluid Sci. 32 (2008) 1188–1191.
[32] I.R. Jones, D.H. Edwards, An experimental study of the forces generated by the collapse of transient cavities in water, J. Fluid Mech. 7 (1960) (1960) 596–609.
[33] B.L. Henke, E.M. Gullikson, J.C. Davis, X-ray interactions: photoabsorption, scattering, transmission, and reflection at E = 50-30000 eV, Z = 1-92, At. Data Nucl. Data Tables 54 (2) (1993) 181–342.
[34] Y. Wang, H.T. Li, Z. Fan, Oxidation of aluminium alloy melts and inoculation by oxide particles, Trans. Indian Inst. Met. (2012), http://dx.doi.org/10.1007/s12666-012-0194-x. Technical Report.
[35] J. Campbell, Castings, second ed., Butterworth-Heinemann, 2003. pp. 17–69.
[36] S.W. Ohl, A. Shrestha, B.C. Khoo, A. Kishen, Characterizing bubble dynamics created by high intensity focused ultrasound for the delivery of antibacterial nanoparticles into a dental hard tissue, Proc. Inst. Mech. Eng. H 224 (2010) 1285–1296.
[37] D. Pavard, E. Klaseboer, S.W. Ohl, B.C. Cheong, Removal of particles from holes in submerged plates with oscillating Bubbles, Phys. Fluids 21 (2009) 083304.
[38] E.J. List, Turbulent jets and plumes, Ann. Rev. Fluid Mech. 14 (1982) 189–212.
[39] I. Tzanakis, M. Hadfield, I. Henshaw, Observations of acoustically generated cavitation bubbles within typical fluids applied to a scroll expander lubrication system, Exp. Therm. Fluid Sci. 35 (2011) 1544–1554.
[40] C.T. Hsiao, A. Jayaprakash, A. Kapahi, J.-K. Choi, Georges L. Chahine, Modeling of material pitting from cavitation bubble collapse, J. Fluid Mech. 755 (2014) 142–175.
[41] Munson, Young, Okiishi, Fundamentals of Fluid Mechanics, fourth ed., John Wiley and Sons, Hoboken, 2002. p. 353.
[42] R. Mutharasan, D. Apelian, Filtration: a melt refining method, JOM 32 (1980) 14–19.